Article

Materials with magnetic iron nanoparticles for additive manufacturing

Rocío Redón*[1], Miriam Avila-Aviles[1], Leopoldo Ruiz-Huerta[1,2], Herlinda Montiel[1], Alex Elías-Zúñiga[2,3], Lucy-Caterine Daza-Gómez[1] and Oscar Martínez-Romero[2,3]

[1] Instituto de Ciencias Aplicadas y Tecnología, Universidad Nacional Autónoma de México, Cd. Universitaria, C.P. 04510, Coyoacán, Ciudad de México, México 1; rredon@unam.mx

[2] National Laboratory for Additive and Digital Manufacturing, MADiT, Mexico; leoruiz.unam.mx; leoruiz@unam.mx

[3] Department of Mechanical Engineering and Advanced Materials, Institute of Advanced Materials for Sustainable Manufacturing, Tecnológico de Monterrey, Av. Eugenio Garza Sada Sur 2501, Monterrey 64849, Nuevo León, México; oscar.martinez@tec.mx

* Correspondence: rredon@unam.mx (RR); oscar.martinez@tec.mx (OMR) Tel.: (+52 5556228602, ex 1207; +52 8110170048)

Abstract: Additive Manufacturing and nanotechnology have been used as basic tools for the manufacture of nanostructured parts with magnetic properties to expand the variety of applications in additive processes by tank photopolymerization. Magnetic cobalt ferrite ($CoFe_2O_4$) and barium ferrite ($BaFe_{12}O_{19}$) nanoparticles with the size distribution of average value D_{TEM} of 12 ± 2.95 nm and 37 ± 12.78 nm, respectively were generated by hydroxide precipitation method. The dispersion of the nanoparticles on commercial resins (Anycubic Green and IRIX White resin) was obtained by mechanochemical reactions carried out in an agate mortar for 20 minutes, at room temperature and with limited exposure to light. The product of each reaction was placed in amber vials, also being kept in a box, to avoid contact with light. The photopolymerization process was carried out only at low concentrations (w/w % nanoparticles/resin) since, at high concentrations, there is no formation of pieces due to the high refractive index of ferrites. Raman shift spectroscopy of the final pieces showed that they contain the magnetic nanoparticles, with no apparent chemical changes. The EPR results of the pieces maintain the magnetic properties and apparently, they are not modified during the photopolymerization. Although significant differences were found in the dispersion process of the nanoparticles in each piece, we determined that the photopolymerization did not influence the structure and superparamagnetic behavior of ferrite nanoparticles during processing, and the magnetic properties were successfully transferred to the final 3D-printed magnetic obtained piece.

Keywords: Magnetic nanoparticles; cobalt ferrite; barium ferrite; additive manufacturing; VAT Photopolymerization

1. Introduction

Ferrite nanoparticles are characterized by being magnetic materials composed of oxides containing ferric ions as the main constituent. Among its greatest advantages are applicability to higher frequencies, higher heat resistance and higher corrosion resistance. With these interesting properties, various biomedical applications have been found, including imaging, separation, power transformers, environmental remediation, excellent catalysts, and drug delivery. When these ferrites are incorporated into more complex systems such as composites, their magnetic properties are often lost or substantially diminished [1,2].

These kind of materials, composed of ferrite nanoparticles, have potential use in the manufacture of scaffolds for advanced engineering of bone tissue [3], microchips [4] and force sensors [5]. In biomedicine, for example, these composites can be used in the diagnosis of diseases, by visualizing the spatial distribution of magnetic nanoparticles, called magnetic particle imaging (MPI). However,

Preprints (www.preprints.org) | NOT PEER-REVIEWED | Posted: 5 June 2023 doi:10.20944/preprints202306.0268.v1

parts with defined geometries that emulate anatomical structures are required [6]. This can hardly be manufactured with the materials and manufacturing processes that are currently available, since traditional methods require pressure to shape specific geometries. Therefore, it has been expensive or even impossible to fabricate complicated structures of magnetic components that can lead to better performance and efficiency of such devices [7].

For this reason, additive manufacturing (AM) or three-dimensional printing is presented as an alternative for this problem, since it is known for its unprecedented modeling capacity and rapid prototyping that implies the printing of successive layers of materials from 3D model data to manufacture different components, which typically have complex and intricate geometries [8]. The above gives it the potential to instigate a paradigm shift in the way power magnets are designed and manufactured for example. In fact, companies such as General Electric (GE) and Siemens have been developing AM parts with functional materials [9–11].

Within additive manufacturing processes, photopolymerization vat provides superior advantages compared to other AM methods, since it gives better results in terms of precision and complexity of the final parts [12]. Vat photopolymerization is the Additive Manufacturing process in which a liquid monomer contained in a tank is selectively cured by light-initiated photopolymerization. In this process, the build platform descends one layer away into the tank, the material is photopolymerized by light, once this layer has hardened, the build platform descends again to continue with the construction layer by layer. The energy source used to carry out the photopolymerization of the material can be UV light (stereolithography or SLA), laser or direct digital light (structured light using a bitmap to project images). This technology offers the ability to build at high resolutions, but generally building materials are not mechanically resistant [13].

While researchers have experimented with microscale inorganic particles, research combining AM and nanomaterials is still limited. However, some work carried out in the field has shown that the introduction of nanostructures can significantly affect the final characteristics and properties of the manufactured parts. The addition of nanomaterials to AM print media could allow the creation of new composites that possess unique properties and lead to the expansion of additive manufacturing application areas [14],[15]. Specifically, nanofunctionalized magnetic materials can provide greater variety and represent a key to new applications in 3D printing. Because these kind of materials can be used for 3D printing of magnetic actuators for lab-on-a-chip applications [5] or motion sensors [4], for example.

In the present research, the main objective was to manufacture composite materials of the type: nanostructure (($BaFe_{12}O_{19}$ or $CoFe_2O_4$)-resin) for additive manufacturing, preserving the magnetic properties from cobalt and barium ferrites, in the final pieces obtained by AM.

2. Discussion

2.1. Characterization of $CoFe_2O_4$

XRD pattern for the $CoFe_2O_4$, obtained by hydroxide precipitation method, was carried out to determine the crystallinity and different phases (Figure 1(a)). The pattern displays typical peaks corresponding to the crystallographic planes (1 1 1), (2 2 0), (3 1 1), (4 0 0), (5 1 1) and (4 4 0), which are related to the presence of the inverse spinel-type $CoFe_2O_4$ structure, in agreement with card 22-1086 JCPDS-ICDD. The inverse spinel structure of $CoFe_2O_4$ has a lattice parameter a_o= 8.391900 Å and belongs to the space group *Fd-3m* (227). Which consists of a divalent cation (Co^{2+}, Fe^{2+}), a trivalent cation (Fe^{3+}), and a divalent anion (O^{2-}). The cations A and B occupy the octahedral or tetrahedral site of the inverse spinel structure (Figure 1(b)). Using the data of the highest intensity signal of the diffractogram and the Scherrer equation (Provided a reference), the size of the nanoparticles was determined, resulting in an average diameter of 10.36 nm.

Preprints (www.preprints.org) | NOT PEER-REVIEWED | Posted: 5 June 2023 doi:10.20944/preprints202306.0268.v1

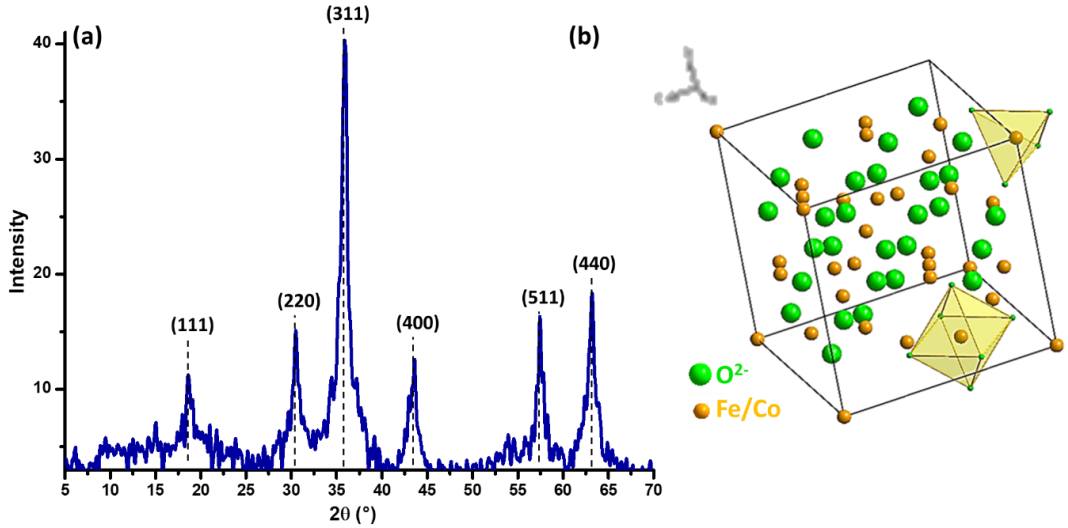

Figure 1. XRD pattern (a) and the representation of inverse spinel-type $CoFe_2O_4$ unit cell (b) obtained with hydroxide precipitation method.

The spectrum obtained by Raman spectroscopy (Figure 2), shows three of the characteristic signals reported in the literature for the inverse spinel-type cobalt ferrite ($CoFe_2O_4$) [16]. Which are assigned for symmetric stretching at tetrahedral sites (A_{1g}); symmetric bending at octahedral sites (E_g) and antisymmetric bending at octahedral sites (T_{1g}) of the crystal structure. Additionally, additional signals are observed around 1300 cm^{-1}, corresponding to a hematite phase (α-Fe_2O_3) [17], as a contaminating phase.

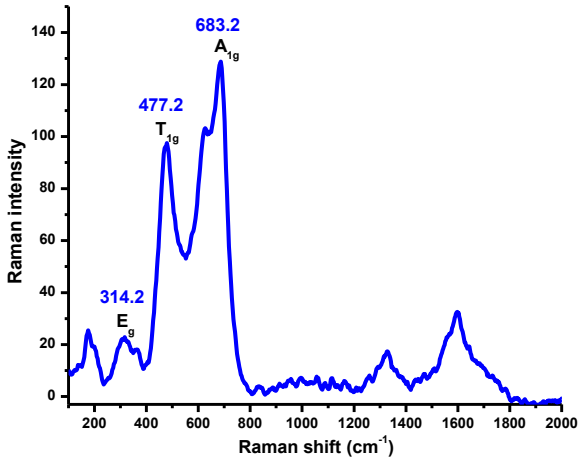

Figure 2. Raman spectra of $CoFe_2O_4$ nanoparticles obtained with hydroxide precipitation method.

HR-TEM images are displayed in Figure 3. It can be observed the presence of $CoFe_2O_4$ with a high degree of agglomeration and a crystal diameter less than 100 nm (Figure 3(a,c)). On the other hand, a size distribution of 20 nanoparticles could be measured, finding that most of the nanoparticles are between 12 and 13 nm in diameter, with an average value D_{TEM} of 12 ± 2.95 nm (Figure 3(b)). This size coincides with that obtained for the size determined by X-ray diffraction (10.36 nm). Using the Fast Fourier Transform (FFT) of the selected area (Figure 3(c)), it was possible to determine the interplanar distances corresponding to the crystallographic planes {2 2 2}, {3 1 1}, {2 2 0} and {4 0 0} of cubic spinel $CoFe_2O_4$ crystal phase.

Preprints (www.preprints.org) | NOT PEER-REVIEWED | Posted: 5 June 2023 doi:10.20944/preprints202306.0268.v1

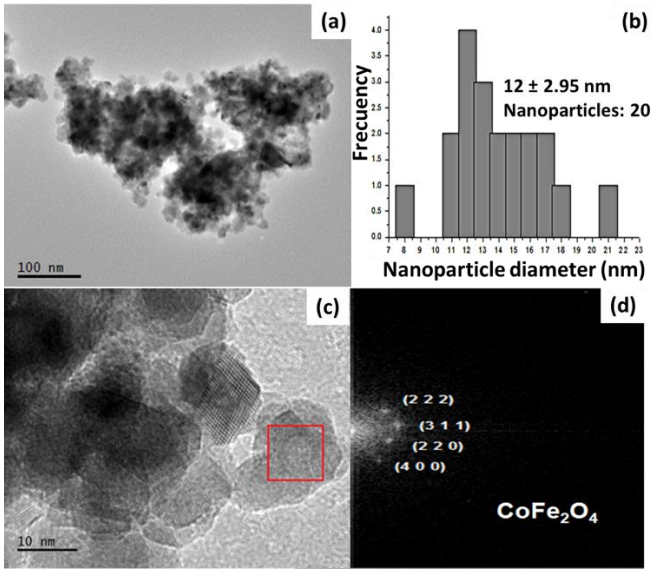

Figure 3. HR-TEM images and its histogram, representing a narrow size distribution of $CoFe_2O_4$ obtained with the hydroxide precipitation method.

In the electron paramagnetic resonance (EPR) spectrum of $CoFe_2O_4$ (Figure 4), part of the characteristic signal of the material can be oberved. Although not complete, due to limitations of the equipment used. The difference between the highest point (it cannot be observed) and the lowest point is called the line width (H_{dc}), which is a qualitative indicator of dipolar magnetic interaction between the magnetic particles of the material; the greater the amplitude of the line width, the greater the concentration of magnetic moments, and the greater the interaction between them. In the case of $CoFe_2O_4$, this signal is very broad and indicates that there is a high dipole energy between the magnetic moments of the particles and, therefore, a strong interaction between them.

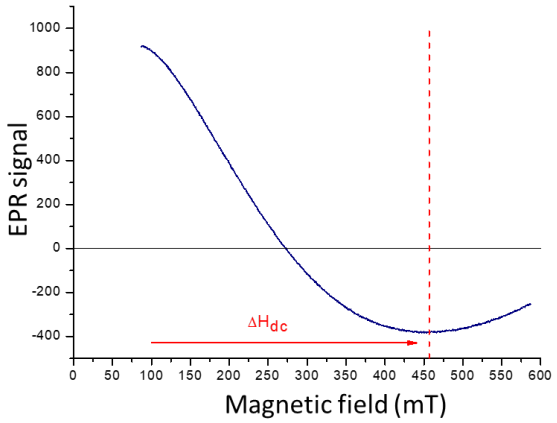

Figure 4. EPR spectra of $CoFe_2O_4$ obtained with the hydroxide precipitation method.

2.2. Characterization of $BaFe_{12}O_{19}$ nanoparticles

The X-ray diffraction pattern (Figure 5) shows the signals corresponding to the crystallographic planes (1 0 2), (0 0 6), (1 1 0), (0 1 7), (1 1 4), (2 0 0), (2 0 3), (2 0 5), (2 0 6), (2 0 9), (2 1 7), (2 0 11), (2 2 0), and (2 4 14) reported in ICDD-PDF N° 01-078-0133 for the crystalline phase of hexagonal barium ferrite ($BaFe_{12}O_{19}$). The hexagonal ferrite structure of $BaFe_{12}O_{19}$ has a lattice parameter a= 5.829, b=5.829, c=23.183 Å and belongs to the space group P63/mmc. The magnetic Fe^{3+} ions occupy five different crystallographic sites: octahedral sites, tetrahedral sites, and trigonal bipyramidal (TBP) sites (Figure 5(b)). Using the data of the highest intensity signal in the XRD pattern and the Scherrer equation, the size of the nanoparticles was calculated, resulting in an average diameter of 49.06 nm.

Preprints (www.preprints.org) | NOT PEER-REVIEWED | Posted: 5 June 2023 doi:10.20944/preprints202306.0268.v1

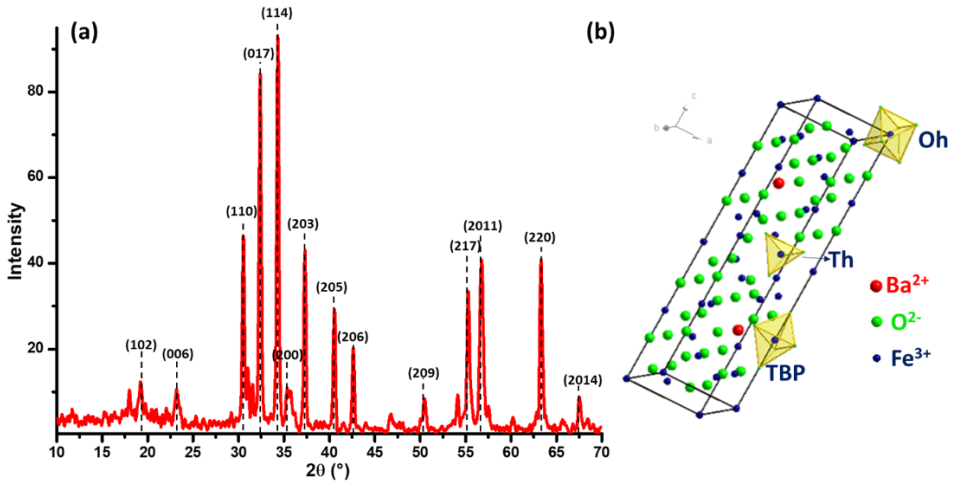

Figure 5. XRD pattern (a) and the representation of hexagonal $BaFe_{12}O_{19}$ unit cell (b) obtained with hydroxide precipitation method.

The spectrum obtained by Raman (Figure 6) shows three of the characteristic signals reported in the literature [16] for hexagonal barium ferrite. These signals correspond to symmetric bending in the spinel block (E_{1g}) at 94.7 cm^{-1}, bending (E_{2g}) at 336.2 cm^{-1} and symmetric stretching at bipyramidal sites (A_{1g}) of the crystal structure at 686.4 cm^{-1}. An additional signal around 1300 cm^{-1} is also observed, which corresponds to an additional phase of hematite (α-Fe_2O_3) [17], as in the case of the cobalt ferrite NPs mentioned previously.

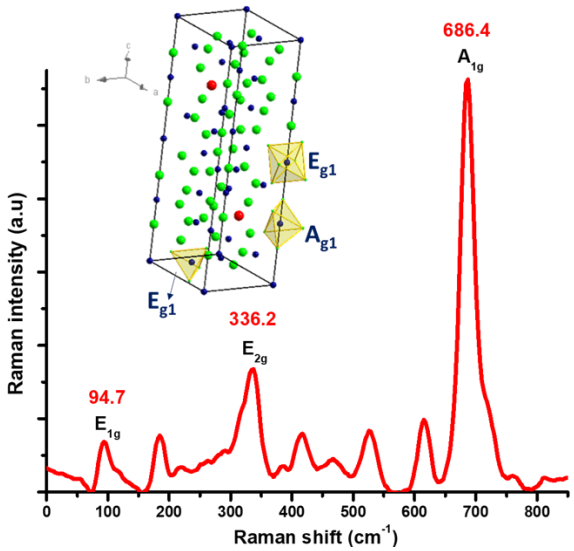

Figure 6. Raman spectra of $BaFe_{12}O_{19}$ nanoparticles obtained with hydroxide precipitation method.

After the structural characterization, a microstructural feature of $BaFe_{12}O_{19}$ was analyzed by TEM (Figure 7). The TEM and HR-TEM images demonstrated that the size of the nanoparticles is less than 100 nm Figure 7(a,c). The particle size distribution of $BaFe_{12}O_{19}$ was between 32 to 42 nm, with an average value D_{TEM} of 37 ± 12.78 nm (Figure 7(b)). This size coincides with that obtained for the size determined by X-ray diffraction of 49.06 nm. Figure 7(d) corresponds to the Fast Fourier Transform (FFT) of the selected area, in which the interplanar distances of the $BaFe_{12}O_{19}$ were identified. The interplanar spacing observed in these micrographs are 2.95, 2.75 and 3.85 Å, corresponding to the {1 1 0}, {0 1 7} y {0 0 6} $BaFe_{12}O_{19}$ family planes, respectively. Additionally, from HR-TEM images, the size distribution of the $BaFe_{12}O_{19}$ NPs was obtained.

Preprints (www.preprints.org) | NOT PEER-REVIEWED | Posted: 5 June 2023 doi:10.20944/preprints202306.0268.v1

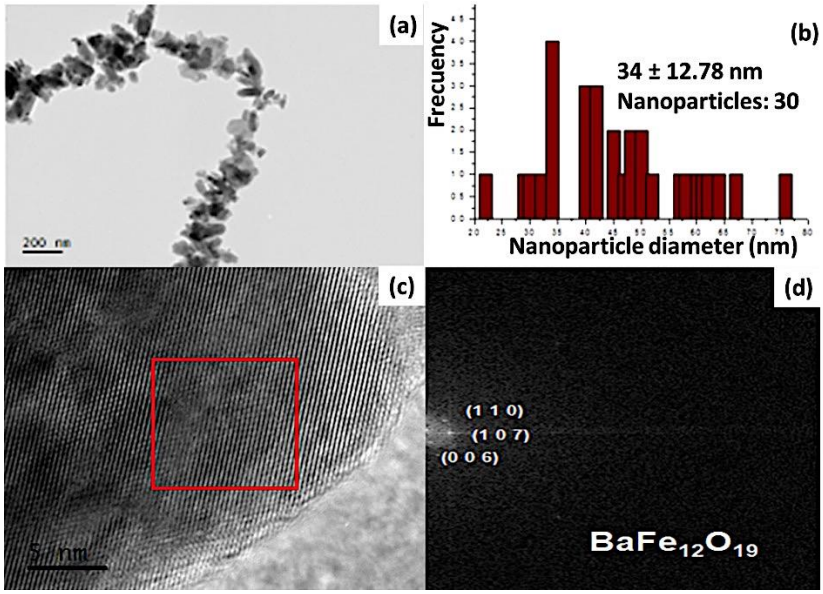

Figure 7. HR-TEM images and its histogram, representing a narrow size distribution of $BaFe_{12}O_{19}$ obtained with the hydroxide precipitation method.

In the EPR spectrum for $BaFe_{12}O_{19}$ (Figure 8), a characteristic signal of the material is observed, which is located from 315.5 to 358.5mT, the difference between these two measurements or line width (H_{dc}), of 43mT, indicates that there is a magnetic dipolar interaction between the nanoparticles of the sample; however, this magnetostatic interaction is less than that obtained in the cobalt ferrite nanoparticles.

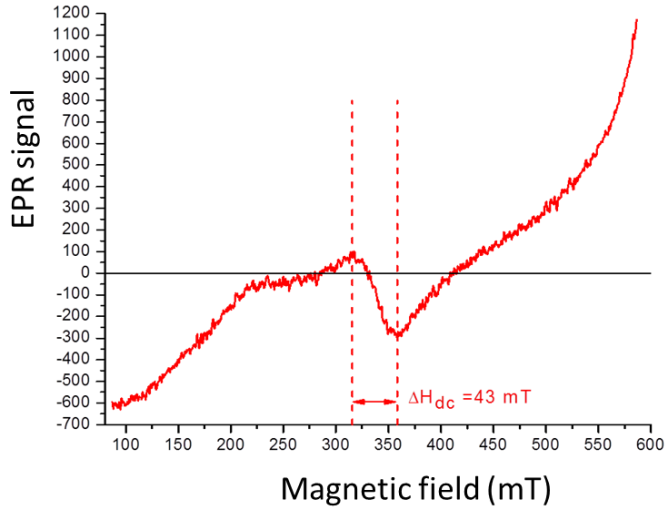

Figure 8. EPR spectra of $BaFe_{12}O_{19}$ obtained with the hydroxide precipitation method.

2.3. Additive Manufacturing Process

2.3.1. Ferrite – IRIX Resin

Figure 9 shows the results of additive manufactured nanostructured samples composed of $BaFe_{12}O_{19}$ and $CoFe_2O_4$–Irix White resin. In both cases, it is notorious that the construction of the cylinders is less and less efficient as the concentration of magnetic nanoparticles increases. The samples with the highest concentration of nanoparticles (NPs) present a certain degree of flaking and are much easier to break than the samples with a lower concentration of NPs; in addition, we had some construction problems at the beginning of the process, probably due to the high refractive index of

Preprints (www.preprints.org) | NOT PEER-REVIEWED | Posted: 5 June 2023 doi:10.20944/preprints202306.0268.v1

the ferrites. (2.3 for $BaFe_{12}O_{19}$ and 2.5 for $CoFe_2O_4$)[13] [14], which did not allow the UV light from the equipment to reach the photosensitive resin correctly once higher concentrations were reached.

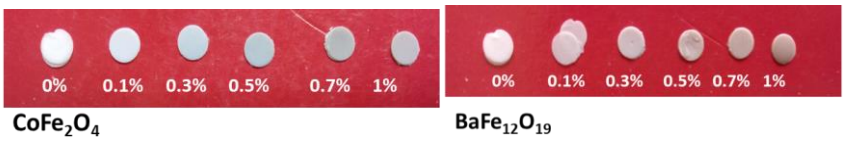

Figure 9. Cylinders built by additive manufacturing by photopolymerization, from 2 different nanostructured ferrites composed of IRIX White ferrite-resin, with different percentages of ferrite.

2.3.2. Ferrite – ANY Cubic Green resin

Figure 10 shows the results obtained in the additive manufacturing of the nanostructured samples composed of $BaFe_{12}O_{19}$ and $CoFe_2O_4$–ANY Cubic Green resin. As with the IRIX resin, the construction of the pieces became less and less efficient as the concentration of magnetic ferrite nanoparticles increased. At a higher percentage of ferrite, the pieces show a certain degree of flaking and are more flexible than the samples with a lower percentage of NPs.

By using these nanostructured materials, only pieces with a concentration of less than 5% w/w of $BaFe_{12}O_{19}$ and concentrations of less than 4% w/w of $CoFe_2O_4$ could be manufactured. Once again, the construction problems were probably due to the high refractive index of the ferrites (2.3 for $BaFe_{12}O_{19}$ and 2.5 for $CoFe_2O_4$) [18]¯[19], which did not allow the UV light from the equipment to reach the photosensitive resin correctly once concentrations were reached (above 5%).

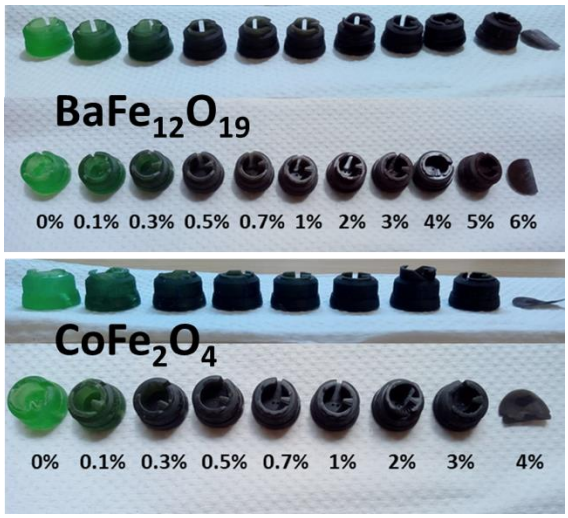

Figure 10. Pieces built by additive manufacturing by photopolymerization, from 2 different nanostructured ferrites composed of IRIX White ferrite-resin, with different percentages of ferrite.

2.3.3. Characterization of composite nanostructured samples

The characterization of the nanostructured samples composed of ferrite-resin was carried out both before and after the additive manufacturing process, in order to know the chemical and magnetic characteristics of the materials, as well as to verify if the nanoparticle magnetic properties are preserved or modified once the process is finished.

Figure 11(a) shows the Raman spectra corresponding to $BaFe_{12}O_{19}$–IRIX resin and $BaFe_{12}O_{19}$–ANY Cubic Green resin nanocomposites. In the spectrum, in addition to the polymer's signals (Figure S1), the three characteristic signals reported in the literature corresponding to $BaFe_{12}O_{19}$ can be observed in both materials. In the case of $BaFe_{12}O_{19}$–IRIX resin, the signals are slightly displaced, suggesting the existence of the interaction between the barium ferrite nanoparticles and the resin, which limits the vibrational modes in the ferrite molecule, displacing them towards the zone of lower

Preprints (www.preprints.org) | NOT PEER-REVIEWED | Posted: 5 June 2023 doi:10.20944/preprints202306.0268.v1

energy; although they remain the same signals for barium ferrite, which indicates that a change in the NPs after the additive manufacturing process is not significant by this technique.

In the case of the $CoFe_2O_4$–IRIX resin and $CoFe_2O_4$–ANY Cubic Green resin nanocomposites (Figure 11(b)), the characteristic signals of the resins are observed, as well as the signals corresponding to $CoFe_2O_4$. The shifting of the ferrite signals is marginal to $CoFe_2O_4$–IRIX resin. This indicates that there is not strong enough interaction between the ferrite and the resin, once the photopolymerization process has been carried out. On the contrary, for $CoFe_2O_4$–ANY Cubic Green nanocomposite, the displacement is significant, indicating a greater interaction between the ferrite and the resin.

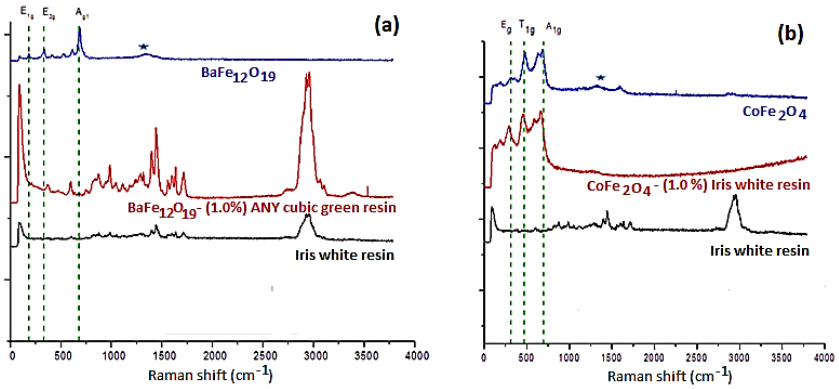

Figure 11. Comparison of Raman spectra of $BaFe_{12}O_{19}$, nanostructured material composed of $BaFe_{12}O_{19}$-IRIX White resin (red spectrum) at 1% m/m, and IRIX White resin (red spectrum).

By comparing the Raman spectra of the both materials, it can be determined that in the case of $BaFe_{12}O_{19}$ nanocomposites and resin signals are present. Therefore, it can be assumed that the distribution of these nanoparticles is in the bulk.

On the contrary, in the $CoFe_2O_4$ nanocomposites it is observed that the signals corresponding to the polymer do not appear in the spectra. Hence, it can be proposed that $CoFe_2O_4$ has a greater interference with Raman laser light than the polymer, thus minimizing the latter's signals in the spectrum, which may indicate that the distribution of the $CoFe_2O_4$ nanoparticles is found on the surface of the pieces.

The EPR analysis of the nanocomposites was carried out, to know the magnetic characteristics of the compounds involved in the experiment (resin, ferrites, nanostructured-composite materials), as well as the changes that the materials may have in their magnetic properties once the additive manufacturing process has been carried out.

Figure 12(a) shows the comparison of the EPR spectra of the nanostructured materials composed of $BaFe_{12}O_{19}$-IRIX White resin prior to the AM process. The concentration of $BaFe_{12}O_{19}$ increases upward. In all the spectra that contain resin, a signal located at 160 mT, assigned to the paramagnetic centers of Fe^{3+}, is observed. In each graph, the characteristic signal of barium ferrite between 315.5 and 358.5 mT is observed, which suggests the presence of $BaFe_{12}O_{19}$ nanoparticles. However, there is a variation in the linewidth of the spectra. It is known that the greater the linewidth amplitude (H_{dc}), the greater the concentration of magnetic moments and the greater the interaction between them. That is, it can be inferred that the particles are closer to each other. By "diluting" the ferrite in the resin, the magnetic moments are separated, and although there is still an interaction between them, by increasing the distance between the magnetic moments, the line width becomes smaller. The variation in the line widths obtained in the spectra (independently of the concentration of nanoparticles) suggests that the dispersion of ferrite in the resin is different for each sample.

In Figure 12(b), the EPR spectra of the $BaFe_{12}O_{19}$–Irix White resin nanocomposites after photopolymerization are shown. Like the samples without treatment, the signal corresponding to the magnetic dipolar interactions of $BaFe_{12}O_{19}$ is observed in all the spectra; however, the line width (H_{dc}) of

Preprints (www.preprints.org) | NOT PEER-REVIEWED | Posted: 5 June 2023 doi:10.20944/preprints202306.0268.v1

each graph is different. This variation in the size of the curve suggests, again, that the dispersion of $BaFe_{12}O_{19}$ nanoparticles is different for each sample even after the additive manufacturing process.

In the case of the piece containing $BaFe_{12}O_{19}$ at 0.5% w/w, a signal corresponding to a splitting or hyperfine interaction is observed. In other words, due to the effect of light, a rearrangement of the electronic levels was generated in the resin, which allows the spin of the nucleus to interact directly with the spin of the unpaired electrons in the resin molecules, whereby it is possible that the sample was exposed to light before the additive manufacturing process.

Comparing the EPR results shown in Figure 12, it was possible to determine that the signal corresponding to the Fe^{3+} ions and the characteristic signal of $BaFe_{12}O_{19}$ are present in all the spectra, both before and after the photopolymerization process. Therefore, both substances, the resin and the nanoparticles, retained their magnetic properties after the additive manufacturing (AM) process.

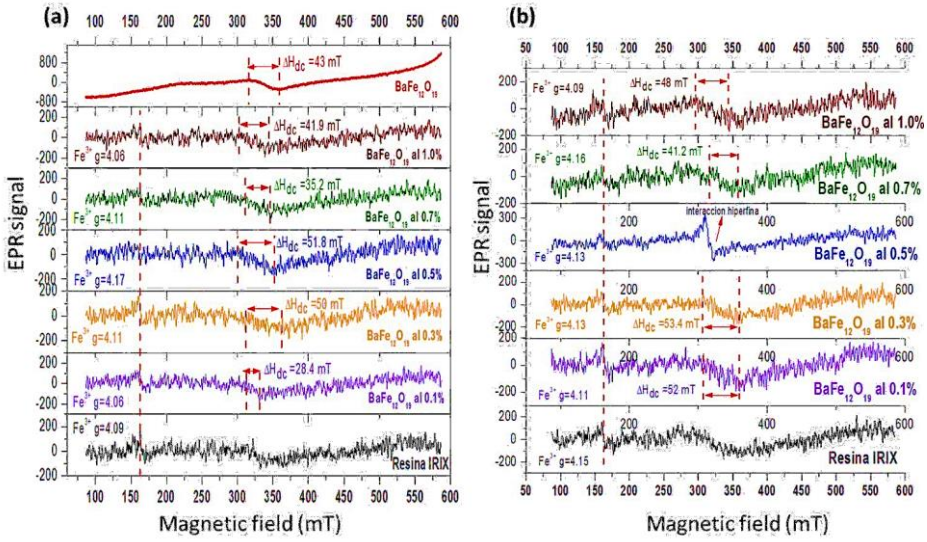

Figure 12. Electron paramagnetic resonance spectra of $BaFe_{12}O_{19}$–Irix White resin samples before (a) and after (b) the additive manufacturing process.

Figure 13(a) shows the EPR spectra of the $CoFe_2O_4$-IRIX White resin nanocomposites before the AM process. In all the spectra containing resin, the signal located at 160 mT, corresponding to the paramagnetic centers of Fe^{3+} is observed. Furthermore, in each graph, the characteristic signal of cobalt ferrite is located between 100 and 460 mT, which reveals the presence of $CoFe_2O_4$ nanoparticles in the samples. In this case, the line width corresponding to $CoFe_2O_4$ could not be obtained, since the signal is incomplete due to the measurement limitations of the equipment used. However, an increase in the intensity of the signal is observed (in all the spectra) as the concentration of NPs increases. This indicates that the higher the concentration of the nanoparticles, the higher concentration of magnetic moments and therefore greater interaction between them, that is, the nanoparticles are closer to each other. By "diluting" the ferrite in the resin, the magnetic moments are separated and the interaction between them diminishes.

Spectra of $CoFe_2O_4$-IRIX White resin nanocomposites after photopolymerization are displayed in Figure 13(b). Again, in all the spectra the signal corresponding to the Fe^{3+} paramagnetic centers of the resin is evident. However, the characteristic signal belonging to the nanoparticles cannot be observed in the spectra. Although in the Raman spectrum for this composite nanostructured material (Figure 11), the peaks associated with the ferrite nanoparticles are observed, these NPs are sufficiently dispersed within the material that the signal corresponding to the magnetic interactions between them are not visible in the spectrum.

Preprints (www.preprints.org) | NOT PEER-REVIEWED | Posted: 5 June 2023 doi:10.20944/preprints202306.0268.v1

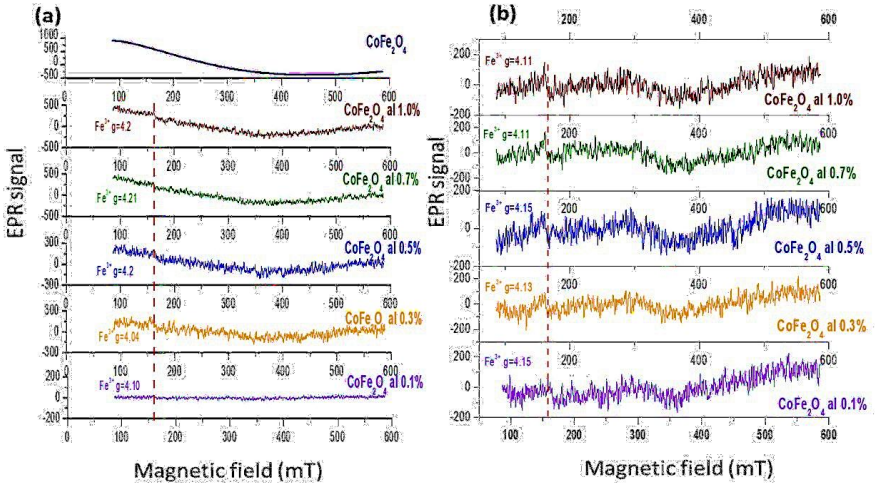

Figure 13. Electron paramagnetic resonance spectra of $CoFe_2O_4$–Irix White resin samples before (a) and after (b) the additive manufacturing process.

3. Materials and Methods

3.1. Materials

The following compounds were purchased from a commercial suplier and were used without further purification: barium nitrate $Ba(NO_3)_2$ (>99%), iron nitrate nonahydrate $(Fe(NO_3)_3)\bullet 9H_2O$) (>98%), cobalt chloride hexahydrate ($CoCl_2\bullet 6H_2O$) (>98%), iron chloride hexahydrate ($FeCl_3\bullet 6H_2O$) (>97%), anhydrous sodium hydroxide (NaOH) (>97%) and methanol (>98%) from Sigma-Aldrich; citric acid monohydrate ($C_6H_8O_7\bullet H_2O$) from Productos Químicos Moterrey; tetrahydrofuran (C_4H_8O) (>99%) and acetone (C_3H_6O) from Reactivos Química Meyer. Deionized tridestilled water was used to wash the products.

3.2. Methods

X-ray diffraction: Siemens Equipment, D5000 Kriotalloflex Diffractometer. Raman shift: Microscope equipment with Raman focal point and WITec Alpha300RA AFM, lase wavelength of 532nm. High Resolution Transmission Electron Microscopy (HR-TEM): JEOL 2000F, operated at 200kV. Electronic Paramagnetic Resonance: Equipment JES-TE300, Jeol-Japan, operating X band. Additive manufacturing to IRIX White resin: Equipment model Prefactory 3 from Envision TEC company, with UV light at 385nm wavelength. Additive manufacturing to ANY Cubic Green resin: Photon equipment from ANY CUBIC company, with UV-LED light at 405nm wave-length.

3.3. Synthesis of $BaFe_{12}O_{19}$ Nanoparticles

The synthesis of barium ferrite was carried out by the hydroxide precipitation method. Iron nitrate ($(Fe(NO_3)_3 \cdot 9H_2O$), barium nitrate $Ba(NO_3)_2$ and citric acid ($(C_6H_8O_7)H_2O$) were dissolved in distilled water in a molar ratio of 12:1:13. The solution is heated to 80°C, with constant stirring for 30 minutes to obtain the coordination compounds: nitrate-citric acid. After this, a 3M NaOH solution is slowly added, keeping the temperature under heating at 80°C and constant stirring for 30 minutes to obtain the hydroxy-citrate complexes of both cations (Fe^{3+} and Ba^{2+}). The brown precipitate is then centrifuged and rinsed alternately with distilled water and methanol, followed by being left in an atmospheric environment to dry. The brown powders are then calcinated at 750°C for 3h.

3.4. Synthesis of $CoFe_2O_4$ Nanoparticles

The synthesis of barium ferrite is carried out by the hydroxide precipitation method. Iron chloride ($FeCl_3\bullet 6H_2O$) and cobalt chloride ($CoCl_2\bullet 6H_2O$) were dissolved in tetrahydrofuran (THF) in a 2:1 molar ratio. Afterwards the solvent is partially evaporated (formation of a green gel of ions dissolved

Preprints (www.preprints.org) | NOT PEER-REVIEWED | Posted: 5 June 2023 doi:10.20944/preprints202306.0268.v1

in THF). Then, a 3M NaOH solution is added to the gel and the reaction was maintain at 80°C and constant stirring for two hours to obtain the metal hydroxides $Co(OH)_2$ and $Fe(OH)_3$. After the hydroxides had been synthetized, an aqueous solution of H_2O_2 (30% wt. % H_2O) is added dropwise and under constant stirring to obtain the cobalt ferrite nanoparticles ($CoFe_2O_4$). Then, the black precipitate is centrifuged and rinsed alternately with tridestilled water and methanol, followed by being left in an atmospheric environment to dry.

3.5. Obtaining nanostructured materials

Nanostructured materials were obtained through mechanochemical reactions from two photosensitive resins: IRIX White (DWS Systems) and Anycubic green (Anycubic) and the previously synthesized and characterized magnetic cobalt ferrite ($CoFe_2O_4$) and barium ferrite ($BaFe_{12}O_{19}$) nanoparticles. The percentages (%w/w) of ferrite used in each of the reactions are shown in tables S1 and S2. Each mechanochemical reaction was carried out in an agate mortar for 20 minutes, at room temperature and with limited exposure to light. The product of each reaction was placed in amber vials, also kept in a box, to avoid contact with light.

3.6. Additive manufacturing process

The AM process was carried out by tank photopolymerization for each of the resin and nanoparticles-resin samples obtained by mechanochemistry. With the nanostructured samples of ferrite and IRIX White resin, cylinders of 5 mm in diameter and 1mm in height were manufactured, through the AM process of VAT photopolymerization, using a UV light at a wavelength of λ = 385 nm. After the construction of each piece, they were washed with isopropanol and dried in an ultraviolet light chamber. On the other hand, with the nanostructured samples of ferrite and ANY Cubic Green resin, the manufacture of complex pieces (base of a chess tower) is carried out through the AM process of VAT photopolymerization, using a UV light at a wavelength of λ = 405 nm. After the construction of the pieces, they were washed with isopropanol and left in an atmospheric environment to dry.

4. Conclusions

Ferrites of barium and cobalt with nanometric size with superparamagnetic regimen, were synthesized by the precipitation method by hydroxides. The magnetic behavior was confirmed by electron paramagnetic resonance, where all samples presented a characteristic signal (315-358 mT for $BaFe_{12}O_{19}$ and 100-450 mT for $CoFe_2O_4$) associated with dipolar interactions between magnetic nanoparticles. In addition, it was possible to determine that the magnetic interaction between $CoFe_2O_4$ nanoparticles is much greater than the magnetic interaction between $BaFe_{12}O_{19}$ nanoparticles.

The photopolymerization process was successfully carried out at low concentrations (m/m%) of nanoparticles (up to 3.0% for $CoFe_2O_4$ and 5.0% for $BaFe_{12}O_{19}$). At higher concentrations, the refractive index of the ferrites precluded the formation of pieces since light is effectively prevented from reaching the photomonomer.

The presence of the crystalline phases of both ferrites in the manufactured pieces was detected by Raman shift spectroscopy, with no apparent chemical changes after the additive manufacturing process. Additionally, a stronger interaction between $BaFe_{12}O_{19}$ and the IRIX White resin was detected.

Finally, according to the results of electronic paramagnetic resonance, the pieces manufactured by the additive manufacturing process have magnetic properties from the nanoparticles used and these magnetic properties apparently do not change during the photopolymerization process; however (according to the variation of the line width) the dispersion of the nanoparticles within each piece is different.

Supplementary Materials: The following supporting information can be downloaded at: www.mdpi.com/xxx/s1, Figure S1: title; Table S1: title; Video S1: title.

Author Contributions: "Conceptualization, formal analysis, investigation, supervision and project administration, R.R; methodology, all authors have the same contribution; resources, R.R. and O.M.R.; writing—original draft preparation, R.R. and L.C.D.G.; writing—review and editing, all authors have the same contribution; funding acquisition, R.R. and O.M.R. All authors have read and agreed to the published version of the manuscript." Please turn to the CRediT taxonomy for the term explanation. Authorship must be limited to those who have contributed substantially to the work reported.

Funding: "This research was funded by PAPIIT-UNAM, grant numbers IN114217,IG100220 and PAPIIT IT102423"; "UNAM Posdoctoral Program (POSDOC)" and "CONACyT", grant number 140617.

Conflicts of Interest: "The authors declare no conflict of interest."

References

1. Trukhanov, A. V.; Tishkevich, D.I.; Podgornaya, S. V.; Kaniukov, E.; Darwish, M.A.; Zubar, T.I.; Timofeev, A. V.; Trukhanova, E.L.; Kostishin, V.G.; Trukhanov, S. V. Impact of the Nanocarbon on Magnetic and Electrodynamic Properties of the Ferrite/Polymer Composites. *Nanomaterials* **2022**, *12*, 868, doi:10.3390/nano12050868.
2. Houbi, A.; Aldashevich, Z.A.; Atassi, Y.; Bagasharova Telmanovna, Z.; Saule, M.; Kubanych, K. Microwave Absorbing Properties of Ferrites and Their Composites: A Review. *J Magn Magn Mater* **2021**, *529*, 167839, doi:https://doi.org/10.1016/j.jmmm.2021.167839.
3. Yang, Z.; Peng, H.; Wang, W.; Liu, T. Crystallization Behavior of Poly(ε-Caprolactone)/Layered Double Hydroxide Nanocomposites. *J Appl Polym Sci* **2010**, *116*, 2658–2667, doi:https://doi.org/10.1002/app.31787.
4. Zhou, B.; Xu, W.; Syed, A.A.; Chau, Y.; Chen, L.; Chew, B.; Yassine, O.; Wu, X.; Gao, Y.; Zhang, J.; et al. Design and Fabrication of Magnetically Functionalized Flexible Micropillar Arrays for Rapid and Controllable Microfluidic Mixing. *Lab Chip* **2015**, *15*, 2125–2132, doi:10.1039/C5LC00173K.
5. Kesner, S.B.; Howe, R.D. Design Principles for Rapid Prototyping Forces Sensors Using 3-D Printing. *IEEE/ASME Transactions on Mechatronics* **2011**, *16*, 866–870, doi:10.1109/TMECH.2011.2160353.
6. Löwa, N.; Fabert, J.-M.; Gutkelch, D.; Paysen, H.; Kosch, O.; Wiekhorst, F. 3D-Printing of Novel Magnetic Composites Based on Magnetic Nanoparticles and Photopolymers. *J Magn Magn Mater* **2019**, *469*, 456–460, doi:https://doi.org/10.1016/j.jmmm.2018.08.073.
7. Chaudhary, V.; Mantri, S.A.; Ramanujan, R. V; Banerjee, R. Additive Manufacturing of Magnetic Materials. *Prog Mater Sci* **2020**, *114*, 100688, doi:https://doi.org/10.1016/j.pmatsci.2020.100688.
8. Peng, E.; Wei, X.; Herng, T.S.; Garbe, U.; Yu, D.; Ding, J. Ferrite-Based Soft and Hard Magnetic Structures by Extrusion Free-Forming. *RSC Adv* **2017**, *7*, 27128–27138, doi:10.1039/C7RA03251J.
9. Fedorov, I.; Barhanko, D.; Hallberg, M.; Lindbaeck, M. Hot Turbine Guide Vane Performance Improvement With Metal Additive Manufacturing at Siemens Energy. In Proceedings of the Volume 2C: Turbomachinery — Design Methods and CFD Modeling for Turbomachinery; Ducts, Noise, and Component Interactions; American Society of Mechanical Engineers, June 7 2021.
10. SIEMENS Industrialize Additive Manufacturing Available online: https://www.siemens.com/global/en/markets/machinebuilding/additivemanufacturing.html (accessed on 18 May 2023).
11. GE Research TECHNOLOGY DOMAIN: Additive Manufacturing Available online: https://www.ge.com/research/technology-domains/additive-manufacturing (accessed on 18 May 2023).

12. Stansbury, J.W.; Idacavage, M.J. 3D Printing with Polymers: Challenges among Expanding Options and Opportunities. *Dental Materials* **2016**, *32*, 54–64, doi:https://doi.org/10.1016/j.dental.2015.09.018.
13. Flores Arias, Q.Y. Síntesis y Caracterización de Materiales Nanoestructurados de Ferrita, IIM UNAM. CDMX, México, 2014.
14. Olga Ivanova, Christopher Williams, T.C. Additive Manufacturing (AM) and Nanotechnology: Promises and Challenges. *Rapid Prototyp J* **2013**, *19*, doi:10.1108/rpj-12-2011-0127.
15. Gao, W.; Zhang, Y.; Ramanujan, D.; Ramani, K.; Chen, Y.; Williams, C.B.; Wang, C.C.L.; Shin, Y.C.; Zhang, S.; Zavattieri, P.D. The Status, Challenges, and Future of Additive Manufacturing in Engineering. *Computer-Aided Design* **2015**, *69*, 65–89, doi:https://doi.org/10.1016/j.cad.2015.04.001.
16. Chandramohan, P.; Srinivasan, M.P.; Velmurugan, S.; Narasimhan, S. V Cation Distribution and Particle Size Effect on Raman Spectrum of CoFe2O4. *J Solid State Chem* **2011**, *184*, 89–96, doi:https://doi.org/10.1016/j.jssc.2010.10.019.
17. MORALES-MORALES, J.A. Síntesis de Nano Polvos de Hematita A-Fe2O3 Por El Método de Precipitación Controlada. *Ciencia en Desarrollo* **2017**, *8*.
18. Erdem, D.; Bingham, N.S.; Heiligtag, F.J.; Pilet, N.; Warnicke, P.; Heyderman, L.J.; Niederberger, M. CoFe2O4 and CoFe2O4-SiO2 Nanoparticle Thin Films with Perpendicular Magnetic Anisotropy for Magnetic and Magneto-Optical Applications. *Adv Funct Mater* **2016**, *26*.
19. Widodo, R.D.; Manaf, A. Physical Characteristics and Magnetic Properties of BaFe12O19/SrTiO3 Based Composites Derived from Mechanical Alloying. *AIP Conf Proc* **2016**, *1725*, 20098, doi:10.1063/1.4945552.